A Critical Review of the Electron-Tunnelling Model of Secondary Ion Formation

Klaus Wittmaack*

GSF – National Research Centre for Environment and Health
Institute of Radiation Protection
85764 Neuherberg, Germany

Abstract

The resonant-electron-tunnelling model of secondary ion formation is based on the assumption that the charge state of an atom departing from the unperturbed surface of a metal is determined by its interaction with the electronic system of the substrate. As a result of the interaction, the height $\varepsilon_a(z)$ of the atomic level and its lifetime, described in terms of the level width $\Delta(z)$, depend strongly on the distance z between the atom and the surface. At large distances $\varepsilon_a(z)$ equals the electron affinity A or the ionisation potential I. The key parameter of the substrate is the work function Φ or Fermi level $\varepsilon_F = -\Phi$. The probability of electron tunnelling from the substrate to the atom or vice versa, i.e. the probability of creating an ion, is controlled by the position of $\varepsilon_a(z)$ relative to ε_F. The probability of survival of the ion on its way to $z \rightarrow \infty$ is determined by the level width $\Delta(z)$ at the so-called crossing distance z_c defined as $\varepsilon_a(z_c) = \varepsilon_F$. Meaningful tests of the tunnelling model have been performed by measuring secondary ion yields $Y^{\pm}$ in dependence of the sample's work function, which was varied in a controlled manner by depositing small quantities of alkali atoms on the surface under study. In accordance with theoretical predictions negative ion yields were found to increase monotonically with decreasing Φ. Positive ion yields of elements with $I < \Phi$, on the other hand, exhibited the predicted decrease with decreasing work function. Previous evaluations of experimental data were based on a simplified version of the tunnelling model according to which $\mathrm{d}\ln P^- / \mathrm{d}\Phi = \text{const}$. The approximation

* E-mail: wittmaack@gsf.de

ignores the observed monotonic change in the slope of $\ln P^-(\Phi)$ and has the additional disadvantage that, on integration, it generates incorrect data for P^-. In this study available experimental data are rationalised without simplifications concerning the Φ-dependence of P^-. The yield saturation frequently observed in negative secondary ion emission from surfaces of very low work function was interpreted as reflecting complete ionisation, i.e. $P^- = 1$. Assuming that $\varepsilon_a(z)$ varies according to the image potential created by the departing ion, experimental $P^-(\Phi - A)$ data were used, for the first time, to determine the z-dependence of the level width which was found to be of the form $\Delta(z) \propto \exp(-\gamma z)$, as often assumed in the literature. Unexpectedly, however, and in contrast to the model, the characteristic inverse distances γ, derived from an analysis of data for various emission energies and angles, turned out to be distinctly different. Qualitatively the same trend was observed with an alternative approximation to $\varepsilon_a(z)$. The importance of γ is evident from the fact that the shape of experimental $P^-(\Phi - A)$ data is determined by this parameter. The apparent variability of γ suggests that the assumption of atom emission from an unperturbed surface is violated by the energetic processes occurring during sputter ejection. The bombardment induced surface perturbations appear to be largely responsible for the lack of agreement between experiment and theory in terms of the velocity dependence of P^-. The deviations from the predicted dependence were found to be moderate in data obtained under bombardment at a low primary ion energy of 0.5 keV. At a relatively high energy of 13 keV, however, a velocity dependence was not evident any more. These observations are in accordance with the idea that the magnitude of surface perturbations will increase with increasing impact energy. The effect of perturbations is also quite pronounced in positive ion emission, in which case P^+ was reported to be almost constant at relatively low emission energies (<8 eV). Furthermore, for $I > \Phi$, the ionisation probability did not approach unity in the limit of infinite velocity. This may be interpreted in terms of the existence of an upper limit in survival probability at small crossing distances (<1.5 Å). Previous attempts to extend the tunnelling model by introducing the concept of a local electron temperature on the order of several thousand Kelvin are discussed.

Contents

1. Introduction

Bombardment of a solid sample with energetic primary ions can give rise to sputter ejection of atoms and molecules from the near-surface region of the target. The ionised particles in the sputtered flux are referred to as secondary ions. The mass and energy of the ejected secondary ions can be determined rather easily by passing them through an appropriate spectrometer. If this is done for the purpose of analysing the composition of a sample, the method is known as secondary ion mass spectrometry (SIMS). The problem in SIMS is that the ionisation probabilities of sputtered particles can vary by up to seven orders of magnitude (Wittmaack, 1998). High ionisation probabilities ($>10\%$) in sputtering of positive and negative secondary are generally observed only with alkali halides or ionic-like compounds such as oxides or nitrides. In order to achieve a high secondary ion signal from elemental targets or alloys, one must chemically alter the composition of the sample at its surface or within the topmost layers. Positive secondary ion yields are maximized if one manages to generate and maintain an oxide layer at the sputtered (receding) surface. For high yields of negative secondary ions one needs to lower the sample's work function as much as possible. To accomplish this goal, the bombarded surface must be covered with sub-monolayer quantities of electropositive elements like alkali metals. These necessary requirements for achieving high secondary ion yields are easy to design conceptually but are often difficult to implement in practice.

The most successful approach to describing the formation of secondary ions is the tunnelling model. Several groups have contributed to the development of this theory (Nørskov and Lundqvist, 1979; Brako and Newns, 1981; Lang, 1983). In its original form the model applies to sputtering from metallic samples. A simplified

version of the theoretical predictions has been tested for negative as well as positive secondary ion emission (Yu, 1981; Yu and Lang, 1983). The key parameter in the experiments was the sample's work function Φ which was lowered in a controlled manner, by up to 3 eV, using step-wise deposition of either Li or Cs. At secondary ion energies exceeding 20 eV, the observed velocity dependence appeared to be in accordance with simplified predictions of the tunnelling model. Other studies into the Φ-dependence of negative ion yields of atoms sputtered from elemental targets, however, did not show a velocity effect (Bernheim and Le Bourse, 1987). Another problem with the tunnelling model is that it predicts unit ionisation probability to be achievable in the limit of infinite emission velocity. However, as shown by an analysis of relevant data, this prediction is generally not in accordance with experimental findings (Wittmaack, 1999a).

In view of these conflicting results it appeared desirable to take another look at the predictions of the tunnelling model. The aim was to evaluate the strength and the limitations of this promising theory in more detail than before.

2. Data Basis

2.1. Introductory Remarks

Before entering into a discussion of experimental results and a comparison with the predictions of any theory of secondary ion formation, it is worth considering the requirements for a meaningful evaluation of data. An important aspect to note is that, with available instrumentation, absolute measurements of the ionisation probability $P^{\pm}$ are very difficult. Early attempts were based on the assumption that (i) the transmission of the employed SIMS instrument can be calibrated accurately and (ii) the energy distribution of the sputtered neutral atoms can be derived from analytical sputtering theory (Vasile, 1983; van der Heide, 1994). These assumptions have been shown not to be justified (Wittmaack, 1982, 1999a). A more reliable approach is to determine energy dependent yields of secondary ions and sputtered neutrals in the same instrument. Such measurements were originally performed using quadrupole based instruments that allowed mass and energy analysis to be carried out with and without ionisation of sputtered neutrals in a radio-frequency plasma (Wucher and Oechsner, 1988). Very recently laser based instruments were developed that have generated rather promising results (Meyer et al., 2003; Mazarov et al., 2006).

An alternative approach to comparing experimental data with theoretical predictions rests on the idea that, in favourable cases, one can vary the experimental parameters over a wide range so that the measured data include the case $P^{\pm} \approx 1$.

There is evidence that, with clean metallic targets this is possible when sputtering alkali metal atoms like Cs from very dilute overlayers, the reason being that Cs features a very low ionisation potential, lower than the work function of many metals. Meyer et al. (2003) compared the yields of Cs^+ secondary ions and post-ionised Cs atoms ejected from sputter cleaned, initially Cs covered silver. At very low residual Cs coverage, mean ionisation probabilities of Cs^+ as high as 0.8 were derived from velocity integrated spectra. At higher Cs coverage the ionisation probability was lower, presumable due to a Cs induced lowering of the sample's work function. The method of varying the work function of the sample by depositing small quantities of alkali metals on the sample surface for the purpose of systematically changing the ionisation probability of secondary ions was pioneered by Yu (1978, 1981, 1984a, 1984b) and subsequently extended by other groups (Prigge and Bauer, 1980; Bernheim and Le Bourse, 1987). The reported data constitute the most important pieces of information that one can use to test the predictions of the tunnelling model of secondary ion formation.

2.2. Relevant Examples of Experimental Data

2.2.1. *Negative Secondary Ions*

Examples of experimental data illustrating the dependence of negative secondary ion yields on the work function of the sample are compiled in Figures 1 and 2. The two sets of data in Figure 1, which relate to the emission of atomic ions from the respective target elements, were obtained under distinctly different conditions. Figure 1a shows results reported by Yu (1982) who used an ultrahigh-vacuum, quadrupole based SIMS instrument. A broad low-current, low-energy Ne^+ ion beam served to generate secondary ions at a low primary ion fluence of about 3×10^{14} ions/cm^2 per data point. Li or Cs atoms were deposited in a stepwise manner to reduce the work function Φ of the initially cleaned Si(111) sample ($\Phi_{0,Si} = 4.6$ eV; all work functions of clean elemental substrates taken from Michaelson, 1977). The work function changes were derived from the current-voltage characteristics of a low-energy electron beam directed at the sample at normal incidence. After each step of work function change, ion yields were recorded at several emission energies, defined by the pass energy of the energy filter. This approach introduces a systematic error because the changes in work function give rise to a corresponding change in the surface potential of the sample relative to the energy filter and the mass spectrometer (Wittmaack, 1983). The geometrical semi-apex angle of ion detection was 19°, i.e. rather large. The secondary ion yields reported in the original publication were converted to ionisation probabilities P^- assuming that the yields saturated at $P^- = 1$. The data are plotted as a function of $\Phi - A$, where A is the electron affinity of the sputtered

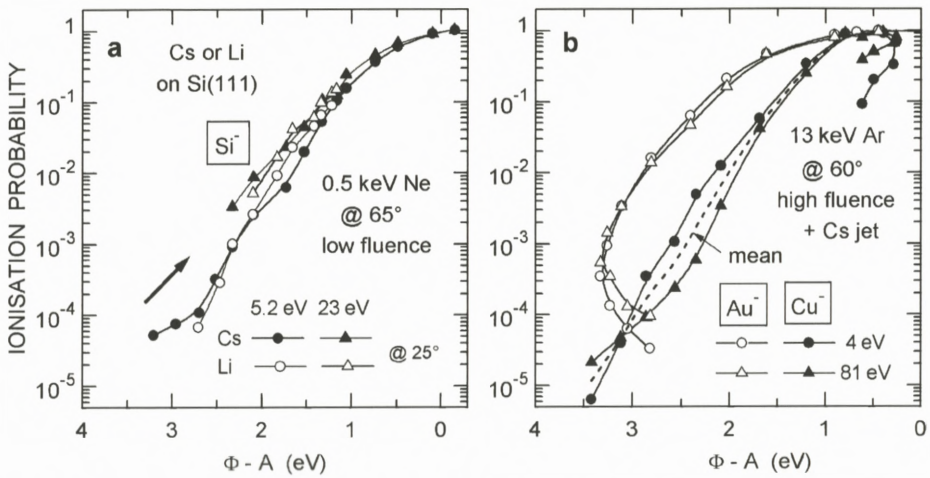

Figure 1. Ionisation probabilities of (a) Si^- and (b) Cu^- and Au^- sputtered from elemental targets (Si, Cu) or a AuCu alloy (Yu, 1982; Bernheim and Le Bourse, 1987). The work function of the targets was varied by depositing Li or Cs. The arrow in (a) denotes the direction of data acquisition. The quoted angles are counted with respect to the surface normal.

atom ($A_{Si} = 1.39$ eV). Note that Φ decreases from left to right. Two aspects of the results in Figure 1a deserve attention. First, within experimental uncertainty, the ionisation probabilities are the same for Li and Cs deposition. Second, at relatively low alkali coverage, i.e. for $\Phi - A > 1.5$ eV, P^- is higher at a (nominal) emission energy of 23 eV than at 5.2 eV. However, the difference is rather small.

The data in Figure 1b were obtained under high-fluence conditions (Bernheim and Le Bourse, 1987), susing a SIMS instrument composed of a magnetic prism and a spherical electrostatic prism. The samples were simultaneously exposed to a beam of Cs vapour and a beam of high-energy Ar^+ ions. Secondary ion yields were recorded after having achieved a dynamical equilibrium between the arrival rate of deposited Cs atoms and the removal rate of Cs atoms sputtered from the sample. The secondary ions were accelerated to the entrance aperture of the secondary ion optics by applying a bias of 3000 V to the target. This approach has the effect that the maximum angle of emission of the secondary ions that were accepted by the spectrometer decreased with increasing emission energy (Wittmaack, 1999a). The changes in work function were derived from the shift of the secondary ion energy spectra associated with the change in the surface potential of the sample relative to the surface potential of the energy analyser. The results for Cu^- emission from polycrystalline Cu ($\Phi_{0,Cu} = 4.65$ eV, $A_{Cu} = 1.23$ eV) are similar to those for Si^- in that the ionisation probability was

found to increase monotonically with decreasing work function. However, a clear dependence of P^- on the emission energy is not evident. If any, P^- is frequently higher at 4 eV than at 81 eV, in contrast to the results for Si^- in Figure 1a. In the data analysis presented below the geometrical mean of the Cu^- data will be used (dashed line).

One should also note that in the Cu^- experiment, the equilibrium Cs coverage was ultimately raised beyond practical limits, i.e. to the point where, after having passed through a well-known minimum in work function observed at about half a monolayer of Cs, Φ increased with increasing Cs coverage, to ultimately approach the work function of bulk Cs ($\Phi_{Cs} = 2.14$ eV). In the region of increasing work function, the Cu^- yield decreased with increasing coverage because the numerous Cs atoms residing at the surface severely inhibited the emission of Cu atoms underneath. The respective data in Figure 1b are ignored in the analysis presented below.

Figure 1b also shows a rather unusual work function dependence of the yields of Au^- sputtered from a $Au_{75}Cu_{25}$ alloy ($A_{Au} = 2.31$ eV). The decrease in work function observed at low Cs fluxes (low "coverage") suggests that due to the high-fluence Ar bombardment most of the Cs atoms were incorporated in the sample rather than staying on the surface, as intended. Under these conditions the method used by the authors for determining the work function seems to break down for currently unknown reasons. Hence the Au^- data are not well suited for a comparison with theoretical predictions. But they are very important because they show, even more convincingly than the Cu^- data, that there was no detectable effect of the secondary ion energy or the emission velocity on the ionisation probability.

The data in Figure 2 are again due to Yu (1981) who investigated the velocity and angular dependence of the yields of O^- ions ($A_O = 1.46$ eV) sputtered from oxygen covered vanadium using the same procedure as in the experiments of Figure 1a. According to Lang (1983) the work function of the oxygen covered V-O sample was 5.2 eV prior to Li deposition. Rather noteworthy is the observation that the ionisation probabilities measured at (nominal) emission energies of 8.3 and 14 eV differ only marginally, if at all, see the data in Figure 2a which relate to an emission angle θ of 55° to the surface normal. A significant velocity dependence was only observed at emission energies exceeding 20 eV, as illustrated by the data for 65 eV. At a constant emission energy of 14 eV, the emission angle was found to have a distinct effect on the ionisation probability, as shown in Figure 2b. The dash-dotted straight line through the experimental data for 14 eV/55° illustrates a linear relation of the form $\ln P^- \propto \Phi$. A closer inspection of the data in Figures 1 and 2, however, shows that the slope $d \ln P^- / d\Phi$ is not constant but changes monotonically as a function of Φ. Nevertheless the approximation

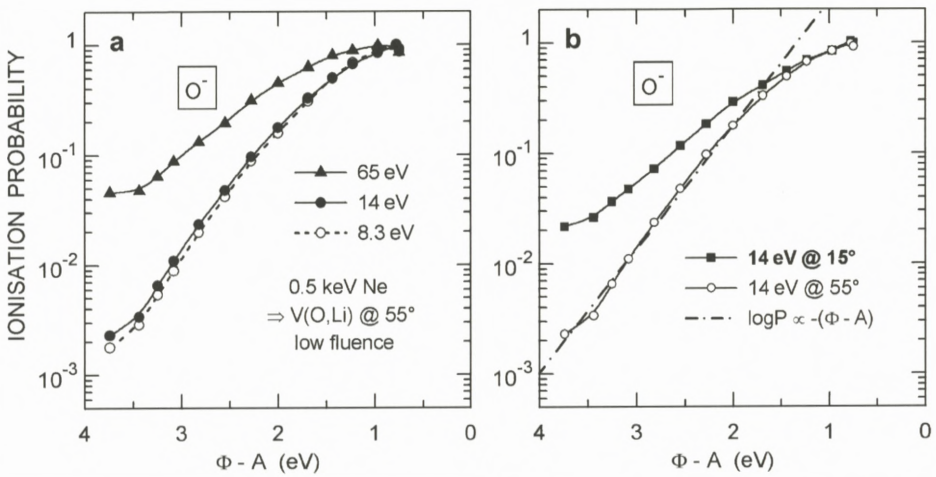

Figure 2. (a) Ionisation probability of O^- sputtered from oxygen on vanadium, for two different emission energies (Yu, 1981). (b) Dependence on emission angle. The dashed line represents a linear fit to log P at low and moderate work function changes.

$d \ln P^-/d\Phi = \text{const}$ was used as the basis for the data evaluation by Yu (1981) and Lang (1983), as discussed in more detail below.

2.2.2. *Positive Secondary Ions*

Experimental data for positive secondary ion emission, suited for a comparison with the predictions of the tunnelling model, are much less abundant than for negative ion emission. Figure 3a shows the work function dependence of the ionisation probability of Cs^+ sputtered from Cs ($I_{Cs} = 3.89$ eV) on polycrystalline Au ($\Phi_{0,Au} = 5.1$ eV), Al ($\Phi_{0,Al} = 4.28$ eV) and Si (Yu and Lang, 1983; Yu, 1984a, 1984b). The data are presented as a function of $I - \Phi$ (note that, in contrast to Figures 1 and 2, Φ decreases from right to left). The small amount of Cs that served as the source of secondary ions was sufficient to introduce a sizable lowering of the work function ($\Delta\Phi = -0.5$ eV for Al and -0.3 eV for Au). Hence the corresponding (first) data points were recorded at $I - \Phi > -1$ eV (compared to $I - \Phi_{0,Au} = -1.21$ eV). Additional changes in Φ were accomplished by depositing Li. The first deposits of Li did not change the initially observed yield of Cs^+, suggesting, in accordance with experimental data of Meyer et al. (2003), that this (maximum) yield corresponded to an ionisation probability $P^+ \approx 1$. This high ionisation probability was retained until Φ had been reduced to the point where $I - \Phi$ for Au and Al had been increased to about 0.6 eV. An additional reduction of Φ resulted in a rapid decrease of the ionisation probability of Cs^+.

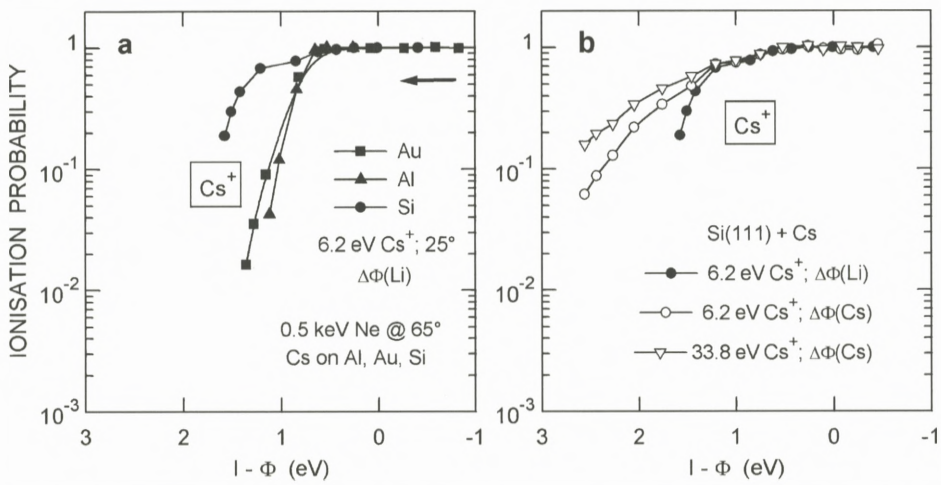

Figure 3. Ionisation probabilities of Cs^+ sputtered from Cs on Au, Al and Si (Yu and Lang, 1983; Yu, 1984a, 1984b). The work function changes were produced by (a) Li and (b) Cs deposition. The arrow in (a) denotes the direction of data acquisition.

The work function dependence of the Cs^+ yields observed in sputtering of Cs from Si exhibited a more complex $(I - \Phi)$-dependence than the data for metal substrates. The initial yield changes observed as $(I - \Phi)$ was raised above 0.6 eV are rather small (see Figure 3b). To produce a more rapid fall-off in Cs^+ yield, $(I - \Phi)$ had to be increased to more than 1 eV. This difference may be related to the fact that Si is a semiconductor. Another problem was encountered when changing Φ by increasing the Cs coverage (rather than by adding Li). As Figure 3b shows, the Cs induced Cs^+ yield changes proceed much more slowly on the $I - \Phi$ scale than the Li induced changes.

3. Concept and Predictions of the Electron-Tunnelling Model

3.1. General Features

The electron-tunnelling model of secondary ion formation involves several important assumptions. (i) The (clean) metal with a work function Φ_0 is at a temperature $T = 0$ K so that all available electron states in the conduction band, considered to be wide, are filled up to the Fermi energy $-\varepsilon_F = \Phi_0$ (see Figure 4). (ii) The sputtering process does not distort the electron distribution, i.e. atoms are emitted from an unperturbed, smooth surface. (iii) The charge state of the departing atom is governed by resonant electron transfer between the atomic level of the atom and

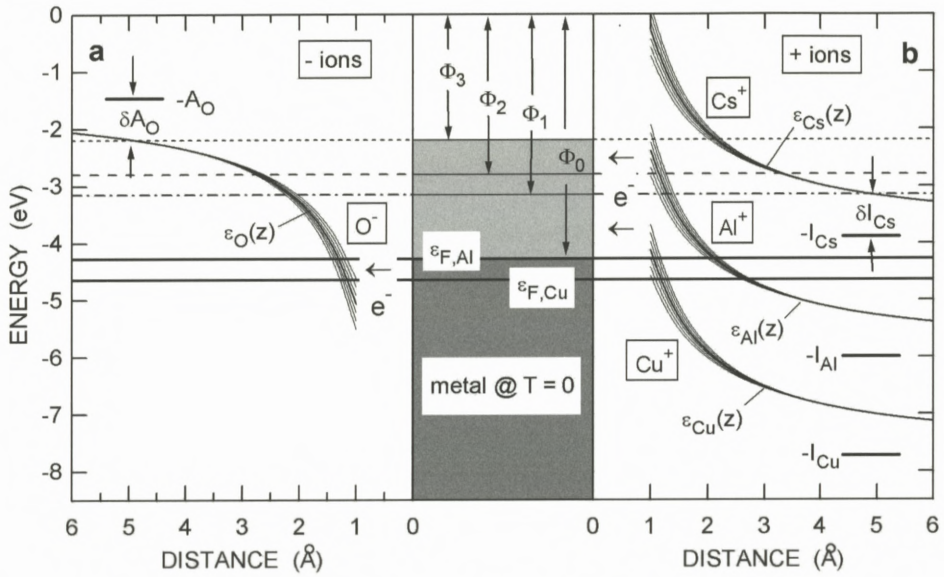

Figure 4. Schematic illustration of the electronic processes occurring as atoms forming (a) negative or (b) positive ions depart from a metal surface. The light-grey areas in the centre denote changes in work function that may be accomplished by the deposition of alkali atoms on the metal surface.

the metal. Electrons can resonantly tunnel in both directions, i.e. from the metal to the atom, thus producing negative secondary ions or neutralising positive ions, or from the atom to the metal, thereby neutralising negative ions or producing positive ions. (iv) The atoms or ions depart from the surface with a constant escape velocity v_n normal to the surface so that time can be easily converted to distance.

The electronic interaction between the atom and the metal has two important consequences: it changes the height $\varepsilon_a(z)$ and the lifetime $\tau(z)$ of the involved atomic level, more so the smaller the distance z between the atom and the surface. The level heights may differ strongly from their respective values at infinity, i.e. from the electron affinity $A = -\varepsilon_A(z \to \infty)$ and the ionisation potential $I = -\varepsilon_I(z \to \infty)$. Very close to the surface accurate calculations of $\varepsilon_a(z)$ and $\tau(z)$ are difficult. Well outside the surface the levels are determined by the image potential $V_{im}(z)$ which shifts $\varepsilon_A(z)$ down and $\varepsilon_I(z)$ up in energy. Examples of $\varepsilon_A(z)$ and $\varepsilon_I(z)$ are sketched, for O^- in Figure 4a and for Cs^+, Al^+ and Cu^+ in Figure 4b. Owing to the finite lifetime $\tau(z)$ of an atomic level near the surface, the level is broadened in energy according to the uncertainty principle, $2\Delta(z)\tau(z) = \hbar$, with $\Delta(z)$ being the half-width of the broadening, indicated by the outermost lines on either side of $\varepsilon_A(z)$ and $\varepsilon_I(z)$. Symmetry with respect to the metal, placed in the

centre of Figure 4, was obtained by allowing the distance in panel (a) to increase from right to left.

The need for the development of the tunnelling model may be appreciated by the results of a simple estimate (Nørskov and Lundqvist, 1979). Let us assume that in course of a sputtering event a secondary ion has been formed somehow. In the immediate vicinity of the surface, the width of the atomic level amounts to about 1 eV or more (see below). This width corresponds to a lifetime $\tau = 2\hbar\Delta \approx 3 \times 10^{16}$ s so that an ion departing from the surface at a normal velocity $v_n = 1$ cm/μs $= 1$ Å/10^{-14} s can travel, on average, only $\tau/v_n \approx 0.03$ Å before being neutralised. Hence the ionisation probability will be very small.

To circumvent this problem, the tunnelling model assumes that, on its way from the surface, the escaping atom can be ionised by resonant tunnelling of an electron from the substrate to the atom, thus creating a negative ion. For this to happen the affinity level must face occupied states in the metal. As the generated ions depart further from the surface, the affinity level increases to cross ε_F at some distance z_c, referred to as the crossing distance. The survival probability at distances $z \geq z_c$, and hence the probability of detecting the ion at large distances ($z \to \infty$), is determined by the lifetime at these distances. In the case of O emission from clean Al or Cu, for example, $\Delta(z)$ is still quite large at z_c (see Figure 4a) so that the ionisation probability is small. If, however, the work function of the sample is gradually reduced, from Φ_0 to Φ_1 or Φ_2, the crossing distance increases. As a result, not only electron tunnelling to the oxygen atom can occur over a wide range of distances from the surface but also the survival probability increases strongly due to the reduced level width (longer lifetime). At some crossing distance the lifetime will be large enough so that essentially all O^- ions formed by resonant tunnelling will be able to survive neutralisation, i.e. tunnelling of an electron from an O^- ion back to empty states above ε_F is then unlikely to occur. In Figure 4a this is assumed to be the case once the work function has been reduced to Φ_3. At that point the affinity level is still well below $-A_O$, by $\delta A_O = \Phi_3 - A_O$.

A different situation is encountered when sputtering Cs from a very thin overlayer of Cs on a metal, as illustrated in Figure 4b. In that case the conditions for secondary ion formation are ideal. Cs features the lowest ionisation potential of all elements, well below the work function of clean Al or Cu. Since $I_{Cs} < \Phi_0$, Cs atoms departing from the surface will always face empty state in the metal so that electrons can tunnel from a Cs atom to the metal at all distances. Hence essentially all sputtered Cs atoms should be able to escape as Cs^+ ions (ionisation probability $P^+ = 1$). The ideal situation changes if the Cs (or Li) coverage is raised to the point where the work function is reduced to Φ_1 or even less. In this range of work

functions, Cs^+ ions formed at small distances will face occupied states in the metal as soon as their separation from the surface exceeds z_c. Therefore, the ionisation probability is expected to decrease rapidly as the work function is reduced below a critical level.

In terms of very low ionisation probability, Cu^+ emission from clean Cu is similar to O^- emission from Cu. With an ionisation potential $I_{Cu} = 7.73$ eV, the condition $-\varepsilon_{I,Cu} < \Phi_{0,Cu}$ applies only at rather small crossing distances z_c, around 1 Å or so, where the survival probability of Cu^+ ions is very small. At distances $z > z_c$, a Cu atom departing from a clean Cu substrate will always face occupied states in the metal from which it was emitted. Hence there is no possibility to form an ion by electron tunnelling from the atom into the metal. The probability for survival would become even smaller if the work function is reduced by depositing alkali atoms.

The third example in Figure 4b, i.e. Al^+ emission from polycrystalline Al ($I_{Al} = 5.99$ eV) constitutes an intermediate case in that $\varepsilon_{I,Al}$ crosses ε_F at a moderate distance $z_c \approx 2$ Å from the surface. Therefore, the survival probability of Al^+ ions generated at $z \leq z_c$ by electron tunnelling from the atom to the substrate is expected to be significantly larger than in the case of Cu^+ emission from Cu.

At this point it is important to note that the well-known enhancement in the ionisation probability of positive (and negative) secondary ions due to surface oxidation of metals and semiconductors (Wittmaack, 1977, 1998) cannot be explained by the tunnelling model. In fact, the pronounced yield enhancement has been observed independent of whether oxidation caused the work function to increase or decrease (Blaise and Slodzian, 1973). Bond breaking was suggested to explain the observed phenomena. In what follows, the effect of oxide formation on the ionisation probability will not be covered.

3.2. Basic Formalism for Negative Ion Formation

In quantitative terms, the ionisation probability P^- calculated in tunnelling theory equals the probability that an atom with the affinity level $|a\rangle$ filled at times $t < t_c$, i.e. before the ion reaches the crossing distance $z_c = z(t_c)$, will survive neutralisation at $t > t_c$, i.e. at $z > z_c$. The probability $\eta(t)\,\mathrm{d}t$ for survival in the time interval $(t, t+\mathrm{d}t)$ is related to the probability $w(t)\,\mathrm{d}t = \mathrm{d}t/\tau(t) = 2\Delta(t)\,\mathrm{d}t/\hbar$ for electron tunnelling back to the substrate as $\eta(t)\,\mathrm{d}t = 1 - w(t)\,\mathrm{d}t = 1 - 2\Delta(t)\,\mathrm{d}t/\hbar$. With the assumption of a constant escape velocity, i.e. with $z = v_n t$, P^- turned out to be (Lang, 1983)

$$P^- \approx P^-(z_c) = \mathrm{e}^{-2\Delta(z_c)/\hbar\gamma v_n}, \tag{1}$$

where γ is a characteristic inverse distance on the order of 1 $Å^{-1}$ and $\hbar$ is Planck's constant. To make use of Equation (1) for predicting ionisation probabilities one needs to know $\Delta(z)$, z_c and γ. In other words, detailed tests of the validity of Equation (1) rest on the availability of theoretical estimates for the input parameters. Here some previously described approaches will be summarised first. Then it is shown that a sizable amount of information concerning the input parameters can be derived directly from the measured work function dependence of the ionisation probability. However, it will be necessary to have detailed *a priori* knowledge concerning the evolution of the affinity level as a function of the atom-surface separation.

3.3. Linear Approximation to $\ln P^-$

In the past, the validity of the tunnelling model has been tested merely on the basis of the straight-line fit to experimental data exemplified in Figure 2b, i.e. by assuming that the complex exponential dependence of P^- on physical parameters of the substrate and the departing atom can be simplified in the form

$$P^-(A, \Phi) \cong \mathrm{e}^{-(\Phi - A - b)/\varepsilon_0}, \tag{2}$$

with ε_0 and b being fitting parameters (note that $P^- = 1$ for $\Phi = A + b$). If Equation (2) applies, the velocity dependence of the ionisation probability, represented by the parameter $\varepsilon_0 \propto v_n$, can be derived from the derivative of $\ln P^-$,

$$\varepsilon_0^{-1} = -\frac{\mathrm{d} \ln P}{\mathrm{d}\Phi} . \tag{3}$$

Lang (1983) used Equation (3) as the starting point for an evaluation of the O^- secondary ion yields from oxygen covered vanadium, as reported by Yu (1981) (see Figure 2). In order to arrive at a theoretical justification for the approximate validity of Equation (2), it was necessary to find a reasonably accurate relation between the work function and the crossing distance. For this purpose an assumption had to be made concerning the z-dependence of the shift, $\delta A(z)$, of the affinity level. The relation between $\varepsilon_A(z)$ and $\delta A(z)$ reads (see Figure 4a)

$$\varepsilon_A(z) = -A - \delta A(z). \tag{4}$$

Lang (1983) used the approximation

$$\delta A(z) = (\Phi - A + E_0)\, \mathrm{e}^{-\alpha z}, \tag{5}$$

where α denotes a characteristic inverse length. E_0 is the affinity level with respect to the Fermi level for the O atom at its equilibrium distance, set to be $z = 0$,

$$\varepsilon_A(0) = \varepsilon_F - E_0 = -(\Phi + E_0). \tag{6}$$

By definition of the crossing distance,

$$\varepsilon_A(z_c) \equiv \varepsilon_F = -\Phi. \tag{7}$$

Hence, with Equation (4),

$$\delta A(z_c) = \Phi - A \tag{8}$$

and, with Equations (4) and (5),

$$z_c = \frac{1}{\alpha} \ln\left(\frac{\Phi - A + E_0}{\Phi - A}\right). \tag{9}$$

Furthermore, Lang (1983) made the common assumption (Nørskov and Lundqvist, 1979) that not only the shift but also the level width $\Delta(z)$ depends exponentially on distance,

$$\Delta(z) = \Delta_0 \, e^{-\gamma z}, \tag{10}$$

where $\Delta_0 = \Delta(z = 0)$. Inserting Equation (10) in Equation (1) yields

$$P^- = \exp\left(-\frac{2\Delta_0}{\hbar\gamma v_n} e^{-\gamma z_c}\right) \tag{11}$$

and, with Equation (9),

$$P^- = \exp\left(-\frac{2\Delta_0}{\hbar\gamma v_n}\left[\frac{\Phi - A}{\Phi - A + E_0}\right]^s\right), \tag{12}$$

with $s = \gamma/\alpha$. Equation (11) exhibits the desired linear dependence of $\ln P^-$ on Φ, provided $s = 1$, i.e. $\alpha = \gamma$, and $E_0 \gg \Phi - A$. The characteristic energy ε_0 derived from Equation (12) according to Equation (3) is

$$\varepsilon_0 = \frac{\alpha\hbar v_n}{2\Delta_0} \frac{(\Phi - A - E_0)^{s+1}}{E_0(\Phi - A)^{s-1}}. \tag{13}$$

Using the same input parameters as Lang (1983), i.e. $\Delta_0 = 1.5$ eV, $\gamma = 1.13$ Å^{-1}, $\alpha = 0.76$ Å^{-1}, and $E_0 = 6$ eV, the ε_0-values derived from Equation (13) are compared in Figure 5a with results obtained by applying Equation (3) to the full range of experimental data. It is evident that the calculated ε_0-values are not constant (16% difference per eV for $\Phi - A$ between 1.5 and 3.5 eV). With few exceptions they differ strongly from the data derived as the derivative of $\ln P^-$. The mean ε_0-values according to Yu (1981), represented by dashed and straight horizontal lines, are in accordance with the results obtained in this study, but only

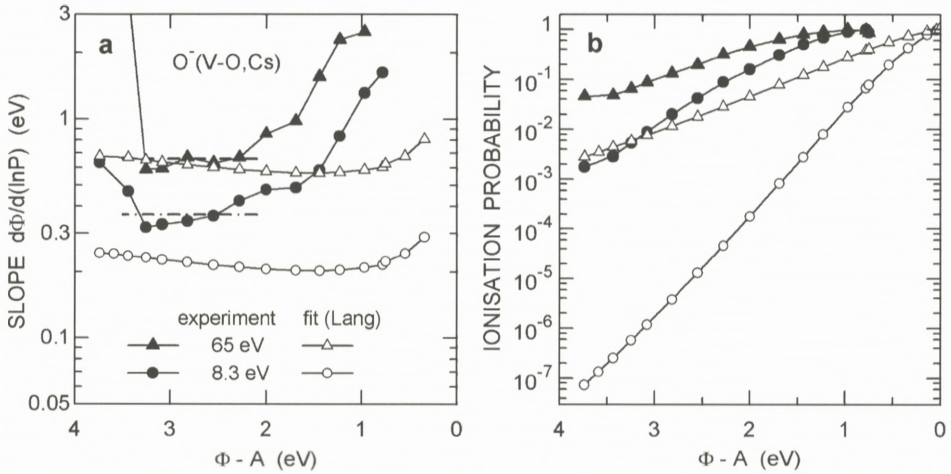

Figure 5. (a) Inverse slope $-1/(\mathrm{d}\ln P/\mathrm{d}\Phi)$ derived from the experimental data and the fit function according to Lang (1983). (b) Ionisation probabilities according to the fit compared with the experimental data. Fit: open symbols; experiment: solid symbols.

within a narrow range of 1 eV or less in terms of work function changes. However, restricting the evaluation to a very narrow range of available data, as done before (Yu, 1981; Lang, 1983) one can hardly arrive at a critical test of the predictions of the tunnelling model.

The poor agreement between the predicted and the experimentally derived ε_0-data can be traced back to the unjustified idea that Equation (2) constitutes a good description of experimental data. As Figure 2b shows, linear sections in graphs of $\log P^-$ (or $\ln P^-$) *versus* Φ can be defined only in narrow ranges of work function changes. Hence ε_0 is neither a constant nor a suitable parameter for describing the work function dependence of the ionisation probability. But this is not the only problem associated with the approach suggested by Lang (1983). Starting with the idea that the derivative of $\ln P^-$ can serve as the leading parameter in the evaluation of experimental data, it should have been clear from the very beginning that one is loosing a potentially important constant contribution to $\ln P^-$ (represented in Equation (2) by $(A + b)/\varepsilon_0$). In the present case this loss of a constant has the dramatic consequence that the ionisation probability calculated according to Equation (12) turns out to be completely wrong, deviating strongly from the experimental data, sometimes by more than four orders of magnitude, as shown in Figure 5b. The reason for the large discrepancy is that the procedure set out to reproduce (only) the slopes $\mathrm{d}\ln P/\mathrm{d}\Phi$. While this has been accomplished in a very approximate manner, but only for $\Phi - A$ between 2 and 3 eV, the absolute values of

P^- do not resemble the experimental data at all. The inevitable conclusion is that the linear approximation to $\ln P^-$ constitutes a completely misleading approach, a scientific meander.

3.4. Rigorous Evaluation

A sufficiently accurate theoretical basis for determining the atom-substrate electronic parameters contained in Equation (1) does not seem to be available presently. Hence it appeared desirable to explore the idea of deriving these parameters from available experimental results. Using Equation (1) we can immediately determine the level width Δ, at least in normalised form and as a function of Φ or $\Phi - A$. Defining an reference level $P_r^- = P^-(\Phi_r)$ which can be chosen arbitrarily, Equation (1) can be rewritten in the form

$$\Delta_r(\Phi) \equiv \frac{\Delta(\Phi)}{\Delta(\Phi_r)} = \frac{\ln P^-(\Phi)}{\ln P^-(\Phi_r)} \,. \tag{14}$$

It is worth noting that, by way of normalisation, the parameters γ and v_n contained in Equation (1) do not appear explicitly in Equation (14). They are contained in hidden form in the experimentally determined parameter $P^-(\Phi_r)$. To proceed we face the same problem as Lang (1983), i.e. we need to correlate the crossing distance with the work function. As an alternative to Equation (5) one can follow Nørskov and Lundqvist (1979) to explore the consequences of the assumption that the shift of the affinity level is determined by the image potential $V_{\mathrm{im}}(z)$,

$$\delta A(z) \equiv V_{\mathrm{im}}(z) = \frac{\mathrm{e}^2}{4(z - z_{\mathrm{im}})} = \frac{3.6}{z - z_{\mathrm{im}}} \,, \tag{15}$$

where z_{im} [Å] denotes the position of the image plane. Using Equations (4), (7) and (15), the conversion of the work function to the crossing distance reads

$$z_{\mathrm{c}} = z_{\mathrm{im}} + \frac{3.6}{\Phi - A} \,, \tag{16}$$

with Φ and A in eV. On this basis the z-dependence of the normalised level width can be determined as

$$\Delta_r(z_{\mathrm{c}}) = \frac{\ln P^-(\Phi)}{\ln P^-(\Phi_r)} \,. \tag{17}$$

Results derived from the data in Figure 2 are presented in Figure 6a. The work function of the alkali-free V-O sample served as the reference point. For simplicity the image plane was assumed to coincide with the origin of the z-scale,

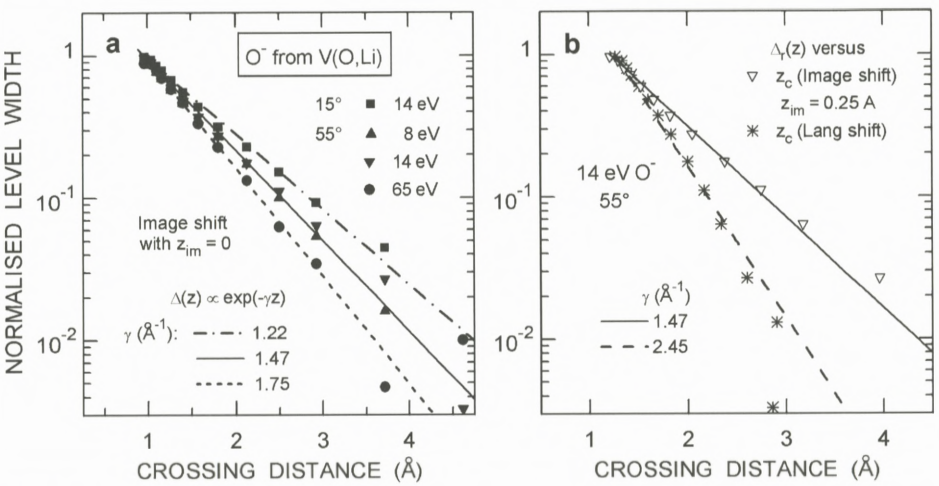

Figure 6. Normalised width of the affinity level of O^- sputtered from oxygen covered vanadium. Data derived according to Equation (17). (a) Crossing distance calculated from the image shift. (b) Comparison of results obtained with the image shift and the shift according to Lang (1983).

$z_{\mathrm{im}} = 0$. The first remarkable result of the evaluation is that, within the limits of accuracy of the data, the affinity level exhibits the commonly assumed exponential dependence on distance, see Equation (10). The increasing scatter of the data for $z_c > 3$ Å is due to the fact that the corresponding P^- values exceed 0.9, in which case Δ_r becomes very sensitive to slight variations of P^-, attributable to statistical errors in the experimental data and uncertainties in the choice of the ion yield corresponding to $P^- = 1$ (note that for $P^- = 1 - \beta$, with $\beta < 0.1$ one can use the approximation $\ln P^- \approx -\beta$). The derived exponential fall-off remains unchanged for $z_{\mathrm{im}} \neq 0$ because $\Delta_r(z)$ is merely shifted by z_{im} in the respective direction, see Equation (16). The evaluated data (solid symbols) can be reproduced quite well inserting γ-values between 1.22 and 1.75 $\mathrm{Å}^{-1}$ in Equation (10), as shown by the straight lines in Figure 6a. Considering the fact that the characteristic inverse distances γ were derived from experimental data for nominal emission energies between 8 and 65 eV and emission angles between 15 and 55°, the different slopes in Figure 6b would imply that γ depends on the normal emission velocity v_n. However, γ is not explicitly contained in the relevant Equation (17). Furthermore, a v_n-dependence of γ would be at variance with the idea that the width of the atomic level depends only on the distance of the atom from the surface. Hence we are led to the preliminary conclusion that a sputtering event involves processes that are not incorporated in the tunnelling model.

One may wonder to what extent the derived data depend on the assumption concerning the z-dependence of the level shift. To address this issue, Figure 6b shows a comparison of normalised level widths derived from the same raw data but by making use of two different analytical descriptions of level shifts, the "image shift" as in Figure 6a (but with $z_{im} \neq 0$) and the "Lang shift" according to Equation (5). In the latter case (the first) 11 data points, out of a total of 14, for P^- between 2×10^{-3} to 0.5 (corresponding to about 90% of the covered $\ln P^-$ scale), are also roughly in accordance with an exponential z-dependence, but with γ as large as 2.45 Å^{-1}. This number is a factor of more than two larger than the estimate of Lang (1983), another piece of evidence supporting the conclusion that the linear approximation to $\ln P^-$ is strongly misleading. As a results of the rapid fall-off of Δ_r, the 11 data points are squeezed together in a rather narrow range of crossing distances between 1.3 and 2.3 Å. With the image-shift concept γ turned out to be much smaller (1.47 Å^{-1}) and the corresponding set of data fall in the range $1.2 < z_c < 3.2$ Å. Note that, to make the two sets of data roughly coincide at small crossing distances, z_{im} had to be set to 0.25 Å. In any case, it is worth noting that all the "action" related to low ionisation probabilities ($P^- < 0.5$) is taking place at distances less than a typical nearest-neighbour distance in a solid.

At this point a direct comparison of the z-dependence of the level shift derived with the two concepts is desirable. Figure 7a shows the Lang shift for two different values of the fitting parameter E_0 and the image shift for two different values of z_{im}. At small crossing distances, i.e. between 1.2 and 2 Å, rather good agreement between the calculated shifts can be obtained for the combination $E_0 = 6$ eV and $z_{im} = 0.25$ Å. Since it has been acknowledged that "far" from the surface the image shift will apply (Lang and Nørskov, 1983), a correction to the image shift may only be necessary below about 2 Å (the term "far" was not defined in any detail). An analytical relation reproducing the Lang shift closely could be achieved by modifying the image shift in the form

$$z_c = \frac{3.4}{\Phi - A} + k[\Phi - A]^m. \tag{18}$$

The thick solid line labelled "fit" in Figure 7a is an example reflecting the case $k = 0.14$ Å and $m = 0.7$. Below 2 Å the resulting shift can be well approximated by the (standard) image shift in combination with $z_{im} = 0.25$ Å.

Extending this exercise on the proper form of the level shift, the next step is to explore the magnitude of the scaling parameter Δ_0 which can be determined from Equation (11) if γ, v_n and z_c are known. Ignoring for the moment the problems associated with the predicted normal-velocity dependence of the ionisation probability, Δ_0 can be written as

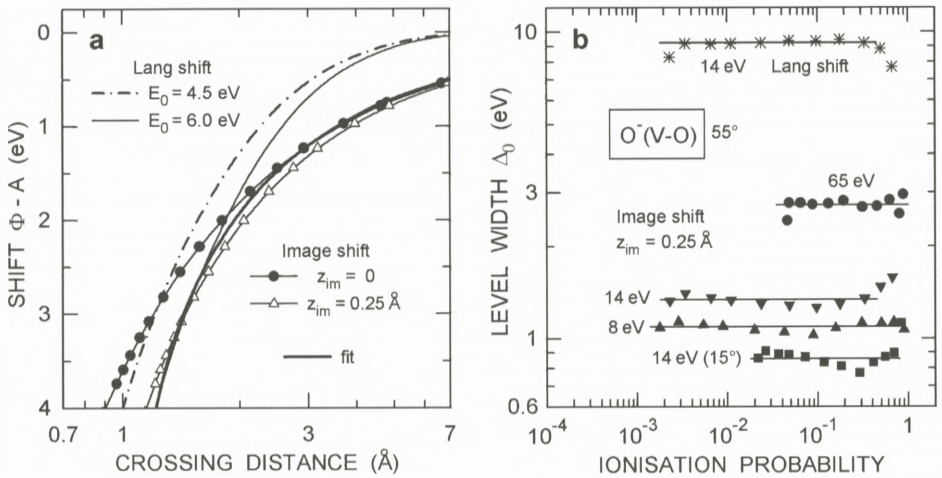

Figure 7. (a) Comparison of the level shifts calculated according to two different approximations. (b) Level width at $z = 0$, derived from experimental data for the ionisation probability of O^- sputtered at different energies.

$$\Delta_0 = -0.5 \ln P^- \hbar\gamma \left(\frac{2E}{M}\right)^{1/2} \cos\theta \, e^{\gamma z_c}, \tag{19}$$

where E and θ are the energy and angle (to the surface normal) of ion emission and M is the ion mass. The results of a data evaluation according to Equation (19) are presented in Figure 7b. Several aspects are noteworthy. First, the results derived for Δ_0 are reasonably constant over a wide range of ionisation probabilities. Deviations are sometimes observed for $P^- > 0.5$. This is either due to the problems of data statistics and calibration, as already discussed with reference to Figure 6, or due to the fact that the z-dependence of Δ_r was not exactly exponential for z_c beyond some critical distance. Second, the derived Δ_0-values exhibit a pronounced dependence on emission energy and angle. Adequate Δ_0-values, which were previously assessed on the basis of surface physical arguments, range between 1 eV (Nørskov and Lundqvist, 1979) and 1.5 eV (Lang, 1983). Hence the results for 8 and 14 eV O^- emission at 55°, obtained using the image shift in combination with $z_{im} = 0.25$ Å ($\langle\Delta_0\rangle = 1.09$ and 1.34 eV, respectively), may be considered quite reasonable. A mean Δ_0-value of 2.73 eV, as derived from the data for emission at 65 eV, appears unreasonably high. This finding may suggest that, in contrast to the interpretation put forward by Yu (1981) and Lang (1983), the most significant deviations from the predictions of the tunnelling model occur at relatively high rather than at low energies. Third, the dependence on the angle

of emission, already observed in deriving Δ_r and γ (Figure 6), is also seen in the data for Δ_0. Emission close to the surface normal (15°) yields smaller numbers for Δ_0 than emission at an oblique angle (55°). Fourth, the Δ_0-value of 9.2 eV, obtained on the basis of the Lang shift for an emission energy of 14 eV, exceeds reasonable numbers by a factor of five. The corresponding number for 65 eV, $\langle\Delta_0\rangle = 27.2$ eV, is completely unrealistic. These results imply that the evaluation of γ and Δ_0-values provides an particularly sensitive test of the validity of the assumed z-dependence of the level shift. The conclusion must be that the Lang shift is not reliable.

Even though proper agreement between the Lang shift and the image shift could be obtained by setting $z_{\mathrm{im}} = 0.25$ Å, the effect of this parameter on the derived values of Δ_0 can serve to assess the possible error in the data of Figure 7b. Using Equation (19) the relation between the two parameters reads

$$\Delta_0(z_{\mathrm{im}}) = \Delta_0(z_{\mathrm{im}} = 0)\, \mathrm{e}^{\gamma z_{\mathrm{im}}}. \tag{20}$$

With $\gamma \approx 1.5$ Å^{-1}, an uncertainty in z_{im} by 0.1 Å corresponds to an uncertainty in Δ_0 by 16%.

3.5. Velocity Dependence

According to the results of Figures 6 and 7 the velocity dependence of the ionisation probability predicted by the tunnelling model may be significantly affected by processes not covered by the underlying assumptions of the model. To discuss the deviations in some detail, we consider the experimental data for 14 eV O^- emitted at 55° from oxygen covered vanadium. The data, shown in Figure 8a as solid symbols, can be reproduced to within typically ±10% or better using Equation (11) in combination with the quoted parameters. This good agreement between experimental data and fit functions was observed for other sets of data as well. Assuming the model to properly predict the velocity dependence of P^-, results expected at some emission energy E_2 can be easily predicted from $P^-(E_1)$ measured at an emission energy E_1,

$$P^-(E_2) = \left(P^-(E_1)\right)^{\sqrt{E_1/E_2}}. \tag{21}$$

Results thus derived from the data for 14 eV are shown in Figure 8a for energies ranging between 5 and 65 eV. The predicted effect of the emission energy on P^- is seen to be quite large, notably at low energies and large work functions.

The procedure according to Equation (21) may also be used to compare the predicted with the measured emission-energy effect on P^-. In Figure 8b the experimental results for 14 and 65 eV at 55° serve as a reference, data measured at

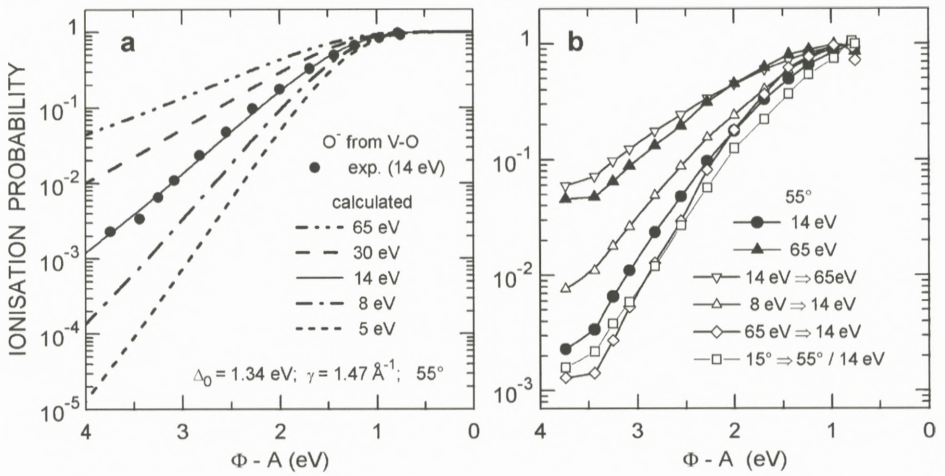

Figure 8. (a) Illustration of the velocity dependence of the ionisation probability P^- predicted by the tunnelling model. The input parameters were derived from a fit to the experimental data for oxygen emission at a nominal energy of 14 eV. (b) Comparison of the measured velocity dependence of P^- (solid symbols) with data obtained using the tunnelling model to convert experimental data from the original emission energy to the reference energies of 14 and 65 eV (open symbols).

other energies were taken as input parameters. The differences between measured and predicted data are significant, sometimes large. The differences are even larger for conversion in more extreme cases like 65 eV → 8 eV (not shown). In analogy to Equation (21) one may also convert data for a given energy and angle to another angle. One example for 15° → 55° is included in Figure 8b. The differences between measured and predicted data, observed at the same nominal energy of 14 eV, imply that the idea of applying corrections to the energy (or velocity) of atom emission cannot resolve existing differences between theory and experiment.

3.6. Some Additional Features of the Tunnelling Model

Even though the tunnelling model may suffer from the fact that some concomitant disturbing effects associated with the sputter emission process are not included, some additional features of the model are worth inspection. Rather than using ratios of $\ln P^-$ to determine the z-dependence of the normalised level width (thus deriving γ), it is worth taking a look at the effect of γ on the shape of $P^-(\Phi - A)$. For this purpose we rewrite Equation (11) as

$$\frac{\ln P^-}{\ln P_r^-} = \mathrm{e}^{\gamma(z_{c,r} - z_c)}. \tag{22}$$

In analogy to Equation (14), Equation (22) does not contain the emission velocity. Furthermore, z_{im} does not appear explicitly in Equation (14). Both parameters are hidden in (the magnitude of) the reference level P_r^-. Using Equation (16) to replace the distance in Equation (22) by the reduced work function, the ionisation probability may be expressed as a function of γ and $\Phi - A$ only

$$P^-(\Phi - A) = \exp\left\{\ln P_r^- \exp\left[3.6\gamma\left(\frac{1}{\Phi_r - A} - \frac{1}{\Phi - A}\right)\right]\right\}. \tag{23}$$

To illustrate the sensitivity of P^- to changes of γ we consider the mean data for Cu^- emission from Cu, which are suited well because they extend over five orders of magnitude in ionisation probability. Somewhat arbitrarily $P_r^-(\Phi_r - A = 2.35\ \mathrm{eV}) = 1.7 \times 10^{-3}$ was selected as the reference level. The results of the fitting procedure are presented in Figure 8a for γ-values ranging between 0.8 and 2.1 $\mathrm{Å}^{-1}$. It is evident that the work function dependence of the ionisation probability is very sensitive to the choice of γ. Hence the optimum value of γ reproducing the experimental data best can be determined rather precisely. In the case of the Cu^- data, $\gamma = 1.2 \pm 0.03\ \mathrm{Å}^{-1}$. The sensitivity of P^- to variations of γ may be considered a proof that resonant tunnelling is the essential process dominating ion formation. If the image potential, with $z_{\mathrm{im}} \neq 0$, is considered to provide a reasonably accurate approximation to the affinity shift, Equation (23) can serve as a very simple means of determining γ directly from experimental data.

As the results of Figure 9a illustrate, γ has a pronounced effect on the way P^- approaches unity. This aspect may be discussed more conveniently by presenting the results on a probability scale, as shown in Figure 9b. The reduced work function $\delta A = \Phi - A$, at which P^- exceeds a certain limit, say 95 or 99%, is seen to depend strongly on γ. More specifically, $\delta A(99\%)$ ranges between 0.38 and 0.78 eV, a difference by as much as 0.4 eV. We note that δA is quite large, amounting to typically one third of the electron affinity of oxygen. The rather large values of δA are due to the fact that the survival probability of a generated ion approaches 100% already at ion-surface distances of about 5 Å (see Figure 4a).

To discuss ionisation probabilities >10% somewhat more, Figure 10a shows O^- data as a function of the crossing distance, with P^- on a linear and z_c on a logarithmic scale. In this kind of presentation the ionisation probabilities have shapes that can be approximated by error functions. Hence the derivatives $P' = \mathrm{d}P/\mathrm{d}z_c$ closely resemble lognormal distributions (see Figure 10b). It was found that, with P according to Equation (11), P' is proportional to the weight function $\Delta_c P$ introduced by Nørskov and Lundqvist (1979),

$$\Delta_c P \equiv \Delta(z_c)P = \frac{\hbar v_n}{2} P'. \tag{24}$$

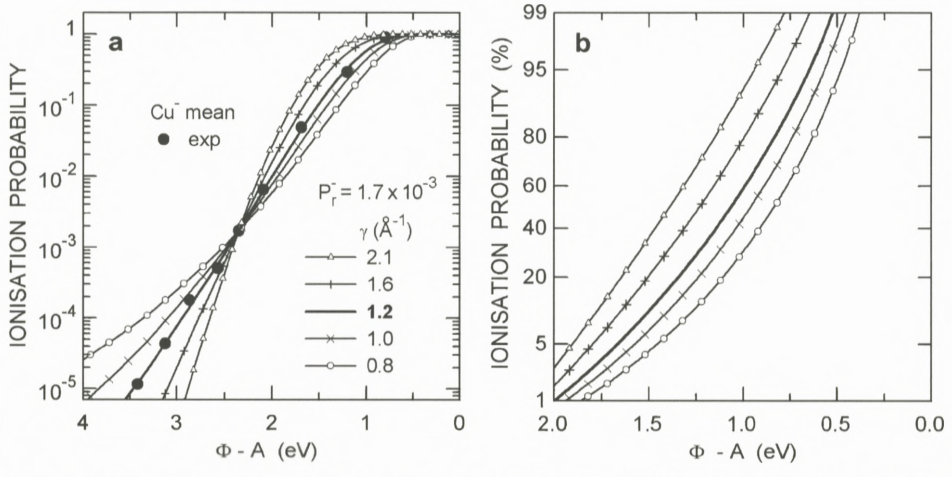

Figure 9. Illustration of the effect of the parameter γ on the work function dependence of the ionisation probability P^-, as predicted by the tunnelling model. The solid symbols represent the mean data for emission of Cu^- from polycrystalline Cu. (a) P^- on a logarithmic scale, (b) on a probability scale. Note the expanded work function scale in (b).

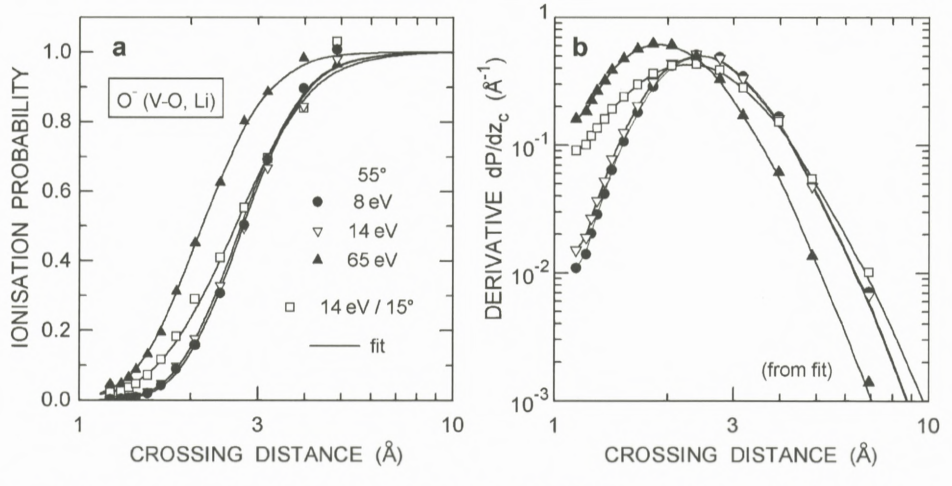

Figure 10. (a) Ionisation probability of O^- *versus* the crossing distance ($Z_{im} = 0.25$ Å). Solid symbols: experimental data for different emission energies, solid lines: fit according to the tunnelling model. (b) Derivatives of the fit functions in (a).

The maximum of the weight function was considered to reflect the "balance" between the excitation probability represented by $\Delta(z_c)$ and the probability $P(z_c)$ that the excitation will survive. The derivatives P' feature a maximum $\hat{P}'$ at

$$z_c(\hat{P}') = -\gamma^{-1} \ln \frac{\hbar \gamma v_n}{2\Delta_0}, \tag{25}$$

with a peak height $\hat{P}' = \gamma/e$. At $z_c(\hat{P}')$ the ionisation probabilities are the same $P(\hat{P}') = 1/e = 0.368$. The deviation from 0.5 reflects the deviation from an exact error function.

3.7. Merging Positive and Negative Secondary Ion Yield Data

One of the particularly interesting aspects of the tunnelling model is that the same formalism can be used to calculate ionisation probabilities of negative as well as of positive secondary ions. Unfortunately, the main body of available experimental data relates only to negative ions. Data for both charge states are rare. An exception are the data of Figures 1a and 3b for the emission of Si^- and Cs^+ from alkali covered Si (Yu, 1982, 1984a, 1984b; Yu and Lang, 1983). The problem with these data is that Si is a semiconductor. The presence of a band gap in this kind of materials introduces uncertainties problems because the definition of an "effective" work function is a subject to ongoing debate (Wittmaack, 1999b). The approach taken here is a pragmatic one: It is assumed that the "effective" work function Φ^* is related Φ, the value determined experimentally, as $\Phi^* = \Phi + \delta\Phi$, with $\delta\Phi$ being a fitting parameter. To illustrate the approach, the normalised level widths derived from the Si^- data in Figure 1a, in analogy to the data in Figure 6, are presented in Figure 11a. With the "standard" assumption, i.e. $\delta\Phi = 0$, the characteristic fall-off parameter γ, derived from the first 11 data points in the range $P^- < 0.25$ is unusually low (0.75 $Å^{-1}$; triangles in Figure 11a). The crossing distance for a moderate ionisation probability of about 0.6 was found to be as large as 7.4 Å. Furthermore, for $P^- \approx 0.9$, the completely unrealistic result $z_c = 36$ Å was obtained (data point not shown in Figure 11a). A much more realistic number, $\gamma = 1.3$ $Å^{-1}$, was derived with $\delta\Phi = 0.6$ eV (circles in Figure 11b). Clearly, this method of deriving $\delta\Phi$ can only be considered a very approximate one. It mainly serves to show that $\delta\Phi > 0$.

It is worth noting that, in contrast to the results of Figure 6, the γ-values derived from the Si^- data in Figure 11a are the same (but the velocity effect seen in Figure 1a is much too small). One presumably important difference between the Si^- and the O^- experiment is that in the former case the ions originated from the substrate, in the latter case from the adsorbed layer. The effect of the

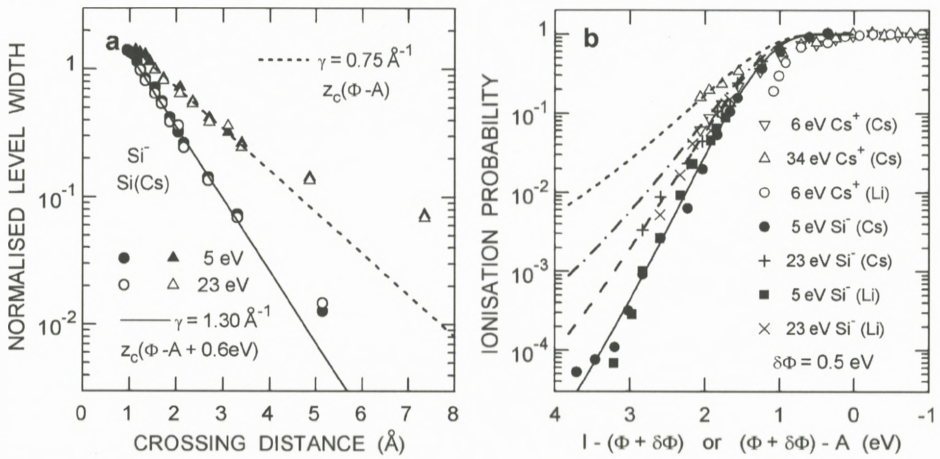

Figure 11. (a) Normalised width of the affinity level of Si^- sputtered from Si. Data derived according to Equation (17). The triangles were obtained assuming the ionisation probability to be controlled by the measured work function. The circles relate to an "effective" work function that is larger by 0.6 eV than the measured value. (b) Comparison of the ionisation probabilities of positive and negative ions sputtered from alkali covered Si. The "effective" work function was assumed to be larger by 0.5 eV than the measured number.

starting position of the analysed ion on the tunnelling probabilty remains to be investigated.

An alternative and probably even more convincing way of assessing the effective work function is to merge ionisation probabilities for positive and negative secondary ions in one graph. Figure 11b shows a compilation of ionisation probabilities for Cs^+ *versus* $I - \Phi^*$ and for Si^- *versus* $\Phi^* - A$. Here the criterion for selecting the optimum value of $\delta\Phi$ was the fall-off in ionisation probability from the level $P^- \approx 1$ which, according to Figure 9, determines γ. For $\delta\Phi = 0.5$ eV the fall-off points for positive and negative secondary ion emission coincided reasonably well (with $\gamma(Si^-) = 1.3$ Å^{-1} and $\gamma(Cs^+) = 1.2$ Å^{-1}). Most of the uncertainty is due the fact that, with available knowledge, no distinction can be made as to whether the Cs^+ data are more reliable for Li or Cs induced work function changes (see Figure 3b). Given these uncertainties, the results of Figure 11b suggest that it is possible to incorporate the ionisation probabilities of positive and negative ions emitted from the same substrate into one graph, thus supporting one of the basic predictions of the tunnelling model. Studies of this kind using metallic substrates would be highly desirable.

3.8. Effect of Surface Perturbations and the Infinite-Velocity Issue

The last issue to be addressed is the origin of the deviations from the tunnelling model which have been quantified, for example, by the results of Figures 6 and 8b. The differences may be due to experimental problems, due to simplifying assumptions of the model or both. On the experimental side there are several uncertainties. In the experiments of Yu (1981, 1982, 1984a), the large acceptance cone, with a geometrical semi-apex angle as large as 19°, prevents a proper definition of emission velocities. Notably at oblique angles of emission (e.g., 55°), the quoted angle may deviate significantly from an appropriate mean value. Additional problems may be brought about by the pronounced angular dependence of the transmission of a quadrupole mass filter (Wittmaack, 1982). With reference to the definition of emission energies, one should note that the surface potential was changing with decreasing work function, and so did the true ion energy (Wittmaack, 1983). Hence it is probably not justified to assign the same energy to all data recorded at different work functions. As to the work of Bernheim and Le Bourse (1987), the issues there are the high primary ion energy, the high bombardment fluence (generating a large surface roughness on polycrystalline metal targets) and the energy dependent maximum angle of ion detection. In future experimental studies attempts should be made to minimise the problems from which the pioneering studies of theses two groups suffered.

On the side of the theory the assumption of a constant emission velocity may cause some problems, as already discussed by Lang (1983). But this aspect does not appear to be capable of explaining the pronounced difference in γ, discussed with reference to Figure 6. Other aspects of the sputtering process, not covered by the assumptions of the tunnelling model, must be of relevance. The notation "surface perturbation" has been used above to describe the origin of the deviations rather vaguely. Nourtier et al. (1988) have considered the sputtering process in more detail in order to explain previously reported ionisation probabilities of Cu^+, which were significantly higher than expected on the basis of the tunnelling model. They questioned the picture of an atom gently desorbing from a flat surface and pointed out that distorted atomic configurations will strongly alter the local electronic structure as well as the relative importance of the various charge exchange channels. Ion scattering in the last collision has also been considered an important deviation from the simple model (Lang, 1983; Lang and Nørskov, 1983; Nourtier et al., 1988). Such aspects and processes could well provide a route to explaining the different γ-values derived in this study. It may also be of interest

to investigate whether the presence of surface inhomogeneities has a significant effect on the model parameters.

One of the frequently discussed predictions of the tunnelling model relates to the question of ionisation probabilities in the limit of infinite velocity. According to Equation (11) we should have $P^-(v_n \rightarrow \infty) = 1$. The same should hold true for P^+. In general, however, as a detailed analysis of literature data has shown, this prediction is at variance with experimental results (Wittmaack, 1999a). Very recent velocity dependent measurements of the yields of secondary ions and laser post-ionised neutrals sputtered from In (Mazarov et al., 2006) support the conclusions of the previous evaluation ($\Phi_{0,\mathrm{In}} = 4.12$ eV; $I_{\mathrm{In}} = 5.79$ eV). The reported ionisation probabilities are depicted in Figure 12 as a function of (a) the emission energy and (b) the inverse emission velocity. The results differ from the predictions of the tunnelling model in two ways. First, the ionisation probabilities observed at low emission energies do not decrease monotonically (and rapidly) but tend to approach some stable level in the limit $E \rightarrow 0$. The low-energy data can be approximated by $P^+ \propto E^{0.05}$, i.e. by a function that increase only marginally with increasing energy. Subtracting this contribution from the raw data, a second, strongly energy dependent contribution is obtained, which is represented by open circles. This contribution (straight dashed line in Figure 12b) exhibits an exponential inverse-velocity dependence, in accordance with the predictions of the tunnelling model. However, the ultimate ionisation probability derived by extrapolation to a vanishing inverse velocity is only $(2 \pm 0.2) \times 10^{-2}$, i.e. much lower than unity. Clearly, the tunnelling model fails to reproduce this observation. The comparatively low ionisation probability derived in the limit of infinite velocity could indicate that, beyond some limit in velocity, the "balance" between ion formation and survival may arrive at an upper limit.

The excess ionisation probabilities observed at In^+ energies below 5 eV may again be indicative of those sputtering events in which atoms (and molecules) were emitted from strongly surface perturbed areas. This kind of distortion appears to be responsible for the observation, reported independently by Wittmaack (1979) and Šroubek (1983), that the ionisation probability in low-energy secondary ion emission from clean samples depends rather strongly on the primary ion energy. The tunnelling model does not include such an energy dependence. Šroubek et al. (1980) were the first to explore the consequences of perturbation due to the ion impact. Using a very simple atomic model, they arrived at ionisation probabilities that increased only very slowly with increasing emission energy, similar to the results in Figure 12a at energies below 5 eV. The excitation of the sample was described in terms of a local electronic temperature generated by the ion impact. The model has been extended more recently (Šroubek and Lörinčik, 2000; Duvenbeck

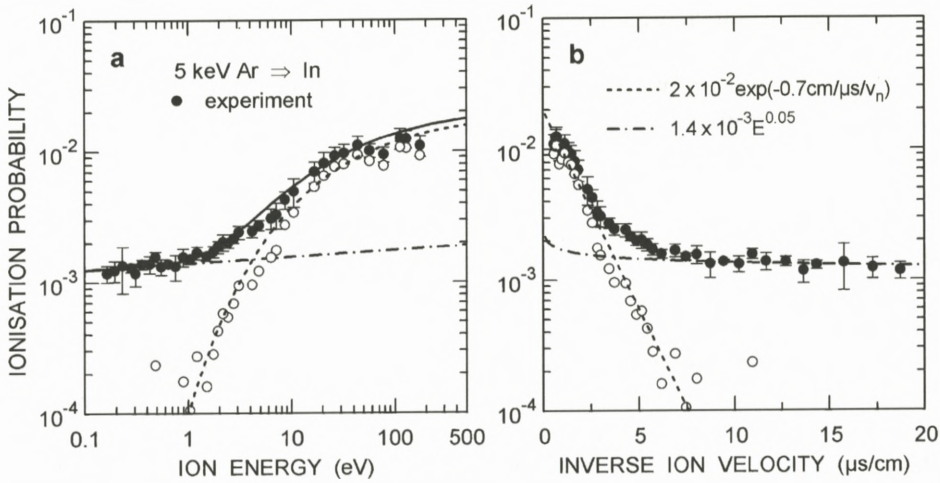

Figure 12. Ionisation probability of In^+ sputtered from clean In, (a) *versus* the energy, (b) *versus* the inverse velocity of the In^+ ions (Mazarov et al., 2006). The dotted lines represent a high-energy fit functions according to the tunnelling model, but with a maximum ionisation probability of only 2×10^{-2}. The dash-dotted line is assumed to represent the contribution of surface perturbations to the total ionisation probability.

et al., 2005; Duvenbeck and Wucher, 2005), but the theory does not seem to have arrived at a mature level yet. It should be noted that, in order to produce effects with a probability on the order of 10^{-3}, only a very small fraction of the sputtering events need to involve strong "perturbation" and "excitation". Molecular dynamics simulations might help to identify the structure of those collision cascades that could act as an additional source of secondary ions.

4. Summary and Conclusions

This study has clarified a number of issues related to the question to what extent the tunnelling model can provide a useful description of secondary ion formation, in qualitative as well as in quantitative form. The strength of the model is that, on principle, it involves a rather simple picture of the electronic processes determining the charge state of an atom that departs from a metallic surface. The results of the experiments performed by Yu (1981, 1984a, 1984b) have provided rather convincing evidence that the basic concept of the model is correct. The evaluation presented here has shown that the ion yields and the derived ionisation probabilities, presented as a function of the alkali induced changes in the sample's work function, are basically in accordance with the predictions of the tunnelling

model, not only for small changes but over the full range of changes. Within experimental uncertainty, the measured ion yields can be reproduced using reasonable input parameters. Inverting the problem, it has been shown for the first time that one can derive relevant input parameters from the experimental data, notably the parameter γ which quantifies the z-dependence of the level width.

There are, however, many unsolved questions relating to the finer details of the tunnelling model. Progress in the theory of electronic interactions between departing atoms and a metallic substrate would be highly desirable, the aim being to calculate the width and the shift of the atomic level from first principles rather than making recourse to reasonable estimates. The calculations should cover the whole range of relevant distances. Of particular importance is the fact that the charge state of a departing atom is determined at distances on the order of or even smaller than a lattice spacing. Hence, intuitively, one would expect the charge states of atoms starting either *on* or *in* the surface to be quite different. Another open questions concerns the absolute value of the ionisation probability. Is it really possible to produce conditions such that all sputtered atoms can escape as ions? This aspect needs to be addressed in much more detail than before.

Undoubtedly, progress in the field will require significant improvements on the experimental side as well. One particular problem with the previous work, both in the low-fluence and the high-fluence studies, is the wide angular distribution accepted by the employed spectrometers. As a result, a well-defined normal velocity cannot be assigned safely to the recorded secondary ions. This uncertainty severely limits the ability to evaluate the predictions of the tunnelling model in terms of the normal-velocity dependence.

The results presented in Figure 12 as well as some other cited results, published more than 20 years ago, imply that perturbations of the surface can give rise to secondary ion yields significantly above the predictions of the tunnelling model. This additional source of secondary ions becomes significant whenever the probability of ion formation due to resonant electron tunnelling is low, typically below 10^{-3}. However, specific limits of validity of the tunnelling model still need to be determined.

References

Bernheim M. and Le Bourse F. (1987): On the velocity dependence for negative ionization of atoms sputtered from cesiated surfaces: An experimental study. Nucl Instrum Meth Phys Res B **27**, 94–103

Blaise G. and Slodzian G. (1973): Effets comparés de l'oxygène sur l'émission ionique et le potentiel de surface des metaux. Surf Sci **40**, 708–714

Brako R. and Newns D.M. (1981): Charge exchange in atom-surface scattering: Thermal versus quantum mechnical non-adiabaticity. Surf Sci **108**, 253–270

Duvenbeck A. and Wucher A. (2005): Low energy electronic excitation in atomic collision cascades: a nonlinear transport model. Phys Rev B **72**, 165408

Duvenbeck A., Šroubek Z. and Wucher A. (2005): Electronic excitation in atomic collision cascades. Nucl Instrum Meth Phys Res B **228**, 325–329

Lang N.D. (1983): Ionization probability of sputtered atoms. Phys Rev B **27**, 2019–2029

Lang N.D. and Nørskov J.K. (1983): The theory of ionization probability in sputtering. Physica Scripta **T6**, 15–18

Mazarov P., Samartsev A.V. and Wucher A. (2006): Determination of energy dependent ionisation probabilities of sputtered particles. Appl Surf Sci **252**, 6452–6455

Meyer S., Staudt C. and Wucher A. (2003): Ionization probability of atoms and molecules sputtered from a cesium covered silver surface. Appl Surf Sci **203–204**, 48–51

Michaelson H.B. (1977): The work function of the elements and its periodicity. J Appl Phys **48**, 4729–4733

Nørskov J.K. and Lundqvist B.I. (1979): Secondary-ion emission probability in sputtering. Phys Rev B **19**, 5661–5665

Nourtier A., Jardin, J.-P. and Quazza, J. (1988): Ionization probability of sputtered atoms: Band-structure and collisional effects. Phys Rev B **37**, 10628–10636

Prigge, S. and Bauer, E. (1980): Static SIMS studies of metal-covered W(110) surfaces. Adv Mass Spectrom **8**, 543–552

Šroubek Z. (1983): Substrate surface excitations and ionisation of particles sputtered from GaAs. Appl Phys Lett **42**, 514–516

Šroubek Z. and Lörinčik J. (2000): Electronic excitations in solids during impact of atomic particles. Vacuum **56**, 263–267

Šroubek Z., Ždánsky K. and Zavadil J. (1980): Ionization of atomic particles sputtered from solids. Phys Rev Lett **45**, 580–583

Van der Heide P.A.W. (1994): Inverse velocity trends in secondary ion mass spectrometry: A new method of quantification? Nucl Instrum Meth Phys Res B **86**, 373–379

Vasile M.J. (1983): The velocity dependence of secondary ions. Nucl Instrum Methods **218**, 319–323

Wittmaack, K. (1977): Secondary ion production due to ion-surface bombardment. In: Tolk N.H., Tully J.C., Heiland W. and White C.W. (Eds), Inelastic Ion-Surface Collisions. Academic, New York, pp 153–199

Wittmaack K. (1979): Secondary-ion emission from silicon bombarded with atomic and molecular noble-gas ions. Surf Sci **90**, 557–563

Wittmaack K. (1982): Design and performance of quadrupole-based SIMS instruments: A critical review. Vacuum **32**, 65–89

Wittmaack K. (1983): The effect of work function changes on secondary ion energy spectra. Physica Scripta **T6**, 71–75

Wittmaack K. (1998): Physical and chemical parameters determining ion yields in SIMS analyses: A closer look at the oxygen induced yield enhancement effect. In: Gillen G., Lareau R., Bennett J. and Stevie F. (Eds), Secondary Ion Mass Spectrometry SIMS XI. Wiley, Chichester, pp 11–18

Wittmaack K. (1999a): The 'infinite velocity method': A means of concentration calibration in secondary ion mass spectrometry? Surf Sci **429**, 84–101

Wittmaack K. (1999b): Ion induced electron emission as a means of studying energy- and angle-dependent compositional changes of solids bombarded with reactive ions: I. Oxygen bombardment of silicon. Surf Sci **419**, 249–264

Wucher A. and Oechsner H. (1988): Emission energy dependence of ionisation probabilities in secondary ion emission from oxygen covered Ta, Nb and Cu surfaces. Surf Sci **199**, 567–578

Yu M.L. (1978): Work-function dependence of negative-ion production during sputtering. Phys Rev Lett **40**, 574–577

Yu M.L. (1981): Velocity dependence of the ionisation probability of sputtered atoms. Phys Rev Lett **47**, 1325–1328

Yu M.L. (1982): Matrix effects in the work-function dependence of negative secondary ion emission. Phys Rev B **26**, 4731–4734

Yu M.L. (1984a): Anomalous coverage dependence of secondary-ion emission from overlayers. Phys Rev B **29**, 2311–2313

Yu M.L. (1984b): On the velocity dependence of secondary ion emission from metallic surfaces. Rad Eff Defects Sol **109**, 259–264

Yu M.L. and Lang N.D. (1983): Direct evidence of electron tunnelling in the ionisation of sputtered atoms. Phys Rev Lett **50**, 127–130